

Review

# Electrochemical Ion Pumping Device for Blue Energy Recovery: Mixing Entropy Battery

Felipe Galleguillos <sup>1,\*</sup>, Luis Cáceres <sup>1,2</sup>, Lindley Maxwell <sup>3,4</sup> and Álvaro Soliz <sup>5</sup>

<sup>1</sup> Departamento de Ingeniería Química y Procesos de Minerales, Universidad de Antofagasta, Av. Universidad de Antofagasta 02800, Antofagasta 1240000, Chile; luis.caceres@uantof.cl

<sup>2</sup> Centro de Investigación Científico y Tecnológico para la Minería (CICITEM), Universidad de Antofagasta, Campus Coloso, Av. Universidad de Antofagasta 02800, Antofagasta 1240000, Chile

<sup>3</sup> Departamento de Química, Universidad de Antofagasta, Av. Universidad de Antofagasta 02800, Antofagasta 1240000, Chile; lindley.maxwell@uantof.cl

<sup>4</sup> Centro de Investigación Avanzada del Litio y Minerales Industriales (CELIMIN), Universidad de Antofagasta, Campus Coloso, Av. Universidad de Antofagasta 02800, Antofagasta 1240000, Chile

<sup>5</sup> Departamento de Ingeniería en Metalurgia, Universidad de Atacama, Av. Copayapu 485, Copiapó 1530000, Chile; alvaro.soliz@uda.cl

\* Correspondence: felipe.galleguillos.madrid@ua.cl; Tel.: +56-9-4235-2163

Received: 21 May 2020; Accepted: 31 July 2020; Published: 11 August 2020



**Abstract:** In the process of finding new forms of energy extraction or recovery, the use of various natural systems as potential clean and renewable energy sources has been examined. Blue energy is an interesting energy alternative based on chemical energy that is spontaneously released when mixing water solutions with different salt concentrations. This occurs naturally in the discharge of rivers into ocean basins on such a scale that it justifies efforts for detailed research. This article collects the most relevant information from the latest publications on the topic, focusing on the use of the mixing entropy battery (MEB) as an electrochemical ion pumping device and the different technological means that have been developed for the conditions of this process. In addition, it describes various practices and advances achieved by various researchers in the optimization of this device, in relation to the most important redox reactions and the cathode and anodic materials used for the recovery of blue energy or salinity gradient energy.

**Keywords:** mixing entropy battery; selective ion capture; insertion electrode; salinity gradient energy; blue energy; prussian blue analogue; battery material; intercalation material

## 1. Introduction

Increasing energy demand and excess pollution, because of the use of fossil fuels, has created the necessity to generate clean energy using available natural resources, thus precluding the use of fuels derived from petroleum. These natural resources include solar, wind, geothermal and biomass being already utilized in various extents. The ocean is another inexhaustible source of renewable energy, highlighting the use of energy from waves, tide, ocean currents, offshore winds, the thermal gradient of the ocean and different salinity concentrations between two solutions, such as seawater and river water [1]. The chemical energy released in the natural mixture between river water flowing into the sea is known as blue energy or salinity gradient energy [2,3]. This chemical or entropy energy dissipates rapidly when river water enters into the sea and is estimated at 2.2 kJ of free energy per liter of fresh water [1,4–10]. The energy produced through the difference in salinity gradients could potentially generate up to 2 TW [5,6,11–15] which is more than 13% [11] of the energy consumed worldwide. The basic principle of a device to recover energy from salinity gradients is the accumulation of charge at

the interface between an electrode and saline water solution as a result of either capacitive phenomena related to the double layer formed at the electrode/solution interface and/or electrochemical reversible reactions at the electrode surface with electroactive species present in saline solutions. The key aspect of this process is the strong dependence between accumulated charge at the interface or the dissociation degree of the electrochemical reactions with the salt concentration in the solution. In order to take advantage of the differing charge densities between two electrodes dipped in fresh and concentrated water solutions, different designs have been proposed. In this review, we summarize the theoretical background of the mixing process, oriented to the mixing entropy battery system, with a focus on existing different designs and operating aspects to achieve a continuous operation.

The objective of this review is as follows: (a) To present the theoretical background and recent advancements in mixing entropy batteries through an overview of the state of the art and most recent technological advances; and (b) To describe materials for these batteries together with major challenges in the technology and the need for fundamental research prior to its world-wide deployment.

## 2. Theoretical Background for Mixing Process

Pattle, in 1954, was the first to propose the mixture between river water and seawater as an interesting alternative renewable energy source, with an electrochemical device called the Hydroelectric Pile [16]. Later, Bert H. Clampitt in 1976, proposed an electrochemical concentration cell design capable of recovering entropy energy from the mixture of solutions with different ionic strengths [17]. More recently, Brogioli in 2009 proposed a novel method based on an electric double-layer (EDL) capacitor called CAPMIX [4].

The mixing entropy battery is a new concept of recovering chemical energy from salinity gradient based on charge storage as chemical energy inside the electrode materials. This process was described by Fabio La Mantia et al. [5] in 2011 as electrochemical capacitors with a faradic charge transfer process [18] delimited by a Nernst potential associated to salt concentration [2,5,6,19].

The “blue energy” that can be extracted from the mingling of fresh water and seawater is best illustrated by its reverse process, “desalination” energy that is required to extract fresh water from seawater. The theoretical non-expansion work that can be produced from mixing a relatively concentrated salt solution  $h$  (seawater) and a dilute salt solution  $l$  (river water), at constant pressure  $p$  and absolute temperature  $T$ , to give a brackish solution  $m$ , is defined by the Gibbs free energy of mixing  $\Delta G_{mix}$  [5,20].

$$\Delta G_{mix} = \Delta G_m - (\Delta G_h + \Delta G_l) \quad (1)$$

Assuming that solutions are ideal dilute, the Gibbs free energy of the mixing process can be calculated just from the change in molar entropy (i.e.,  $\Delta H_{mix} = 0$ ) [18,20]:

$$\Delta G_{mix} = -(n_h + n_l)T\Delta S_{mix,m} - (-n_hT\Delta S_{mix,h} - n_lT\Delta S_{mix,l}) \quad (2)$$

where  $n$  is the amount (moles),  $T$  is the temperature, and  $\Delta S_{mix}$  represents the contribution of the molar entropy of mixing to the total molar entropy of the mixing electrolyte solution (J/mol.K), according to:

$$\Delta S_{mix} = -R \sum_i x_i \ln x_i \quad (3)$$

where  $R$  is the universal gas constant (8.314 J/mol.K) and  $x$  is the mole fraction of component  $i$  ( $i = Na^+, Li^+, Mg^{2+}, Cl^-, H_2O$ ). The mixing entropy battery operates through the Gibbs free energy change, for transferring a species  $i$  from a system 1 to a system 2 ( $\Delta G_{i,1,2}$ ) in isothermal conditions, which can be obtained by adding the Gibbs free energy changes of the two systems separately.

$$\Delta G_{i,1,2} = \Delta G_{i,1} + \Delta G_{i,2} = G_{i,1F} - G_{i,1I} + G_{i,2F} - G_{i,2I} \quad (4)$$

In terms of composition it can be calculated as follows:

$$\frac{\Delta G_{i,1,2}}{RT} = n_{i,1F} \ln(C_{i,1F}) - n_{i,1I} \ln(C_{i,1I}) + n_{i,2F} \ln(C_{i,2F}) - n_{i,2I} \ln(C_{i,2I}) \quad (5)$$

where  $F$  and  $I$  are final and initial conditions of each system, respectively.

On the other hand, the conservation of mass for the transferred species can be represented by the following expression:

$$n_{i,1F} - n_{i,1I} = n_{i,2F} - n_{i,2I} = \Delta n_i \quad (6)$$

Substitution of (6) into (5) and carrying out some mathematical arrangements gives the following:

$$\frac{\Delta G_{i,1,2}}{RT} = n_{i,1F} \ln\left(\frac{C_{i,1F}}{C_{i,1I}}\right) + n_{i,2I} \ln\left(\frac{C_{i,2F}}{C_{i,2I}}\right) + \Delta n_i \ln\left(\frac{C_{i,2F}}{C_{i,1F}}\right) \quad (7)$$

In the present work system "1" represents the brine, and system "2" the recovery solution or fresh water. So, the following approximations can be made:

$$n_{i,2F} - n_{i,2I} \cong n_{i,2F} \quad (8)$$

$$n_{i,1F} - n_{i,1I} \cong 0 \quad (9)$$

This simplifies Equations (7)–(10), used to calculate the Gibbs free energy change, for transferring a species  $i$  from brine to the recovery solution in isothermal conditions.

$$\frac{\Delta G_{i,1,2}}{RT} \cong \Delta n_i \ln\left(\frac{C_{i,2F}}{C_{i,1F}}\right) \quad (10)$$

Finally, the total Gibbs free energy change can be calculated by adding the individual free energy changes for all the species transferred from 1 to 2:

$$\Delta G_{1,2} = \sum_i \Delta G_{i,1,2} \quad (11)$$

Fabio La Mantia proposed using altiplanic brine from Atacama Salar as a concentrated solution (1 M  $LiCl$ ) of electrolyte for harvesting blue energy, achieving satisfactory results [5]. The following expression will be presented in terms of intercalating lithium ions from brine and recovery blue energy in order to make the process of recovery of lithium ions sustainable.

$$\Delta G_{1,2} = 2RT \ln\left(\frac{C_{LiCl,2F}}{C_{LiCl,1I}}\right) \quad (12)$$

For a given amount of moles,  $n$ , of which a fraction  $x$  consists of fresh water with a lithium chloride concentration, and another fraction  $(1-x)$  of brine with a lithium chloride concentration. The theoretical recoverable energy from a mixing process with different saline concentration solutions is calculated as follows:

$$\frac{\Delta G_{mix}}{RT} = C_m \ln(C_m) - x C_l \ln(C_l) - (1-x) C_h \ln(C_h) \quad (13)$$

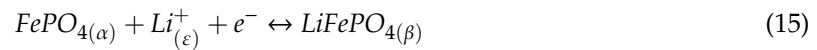
The Gibbs free energy change, between the concentrated solution and the solution with low strength, can be calculated according to the volumetric fraction ( $x$ ) of the concentrated solution, where  $C_m$  is the salt concentration of the final mixture,  $C_l$  is the salt concentration of the solution with low ionic strength, and  $C_h$  is the salt concentration of the concentrated solution [5].

In order to extract the free energy in the water salinity, a faradic pseudo-capacitor systems is used [21]:



In this device, two different electrodes were employed: an anionic electrode of *Ag* metal, which interacts with  $Cl^-$  ions selectively; and a cationic electrode of

$FePO_4$ , which interacts with  $Li^+$  ions selectively. The global reaction (Equation (14)) decomposed in two half-cell electrochemical reactions, and can be written as follows [5]:



where  $\alpha$  is the  $FePO_4$  phase,  $\beta$  the  $LiFePO_4$  phase,  $\varepsilon$  the electrolyte,  $\beta'$  the  $AgCl$  phase and  $\alpha'$  the *Ag* phase. The Nernst potential of the two half-cell reactions with respect to the normal hydrogen electrode (NHE) is given by

$$E_+ = E_+^0 + \frac{RT}{F} \ln \left[ \frac{a_{Li,\varepsilon}}{a_{Li,\beta}} \right] \quad (17)$$

$$E_- = E_-^0 - \frac{RT}{F} \ln [a_{Cl,\varepsilon}] \quad (18)$$

where  $E_+$  and  $E_-$  are the potential of the electrodes,  $E_+^0$  and  $E_-^0$  are the standard potential of the electrodes,  $a_{Li,\beta}$  is the activity of the lithium in the solid phase,  $F$  is the Faraday constant,  $a_{Li,\varepsilon}$  is the activity of the lithium ions in the electrolyte, and  $a_{Cl,\varepsilon}$  is the activity of chloride ions in the electrolyte. The difference between the two potentials is  $\Delta E$ . If the activity of lithium in the solid phase is fixed (no current), one obtains:

$$\Delta E = \Delta E^0 + \frac{RT}{F} \ln [a_{Li(\varepsilon)}] + \frac{RT}{F} \ln [a_{Cl(\varepsilon)}] \quad (19)$$

When a voltage is generated in a device or any part of a circuit, the point of positive potential is said to be at a higher potential than the point of negative potential. The means by which the voltage is generated is said to produce a voltage rise. The theoretical "voltage rise" for this lithium device can be calculated from the Nernst equation, according to the following expression [22]:

$$\Delta E = \frac{RT}{zF} \left[ \frac{C_{Li^+,h} \cdot C_{Cl^-,h}}{C_{Li^+,l} \cdot C_{Cl^-,l}} \right] \quad (20)$$

where  $z$  is the number of electron transferred in the reaction, and subscripts  $h$  and  $l$  refer to concentrated (brine) and diluted (recovery) solutions respectively.

The potential difference between the two electrodes is [23]:

$$E_{Cell} = E_{Cell}^0 + 2 \frac{RT}{F} \ln [C_{LiCl}] + 2 \frac{RT}{F} \ln [\gamma_{LiCl}] \quad (21)$$

where  $E_{Cell}^0$  is the standard cell voltage,  $C_{LiCl}$  is the concentration of  $LiCl$  and  $\gamma_{LiCl}$  is the mean activity coefficient of  $LiCl$ . The dependence of  $\gamma_{LiCl}$  on  $C_{LiCl}$  its described by the Debye-Hückel law [18], which is as follows:

$$\ln [\gamma_{LiCl}] = - \frac{A \sqrt{C_{LiCl}}}{1 + B \sqrt{C_{LiCl}}} \quad (22)$$

where  $A$  and  $B$  are the constants. A mixing entropy battery device consists of a reversible electrochemical system, where the electroactive ions present in the natural solution are pseudo capacitively stored in their respective electrodes. These electrodes work selectively by capturing dissolved ions, where cationic ions ( $M^+$ ) such as the  $Na^+$  (1.02 Å),  $Li^+$  (0.76 Å) or  $Mg^{2+}$  (0.65 Å) [24,25] (or trivalent ions, such as  $Al^{3+}$  and polyvalent ( $B^{n+}$ ) as well) interact with the cathode electrode and anionic ions ( $A^-$ ), such as the  $Cl^-$

ion interacting with the anodic electrode. The CAPMIX and the mixing entropy battery are also known as the Mix Accumulator or AccMix [23].

The mixing entropy battery proposed by Fabio La Mantia operates under a process by which anionic and cationic electrodes, selectively interact with  $Cl^-$  and  $Na^+$  ions in several steps. In step 1, the battery is charged when  $M^+$  and  $A^-$  ions are removed from the respective electrodes in a low ionic strength solution. In step 2, the recovery solution is exchanged for the concentrated solution, generating an increase in cell voltage or open circuit potential; this phenomenon is known as “Voltage Rise” [1,2,4,5,7,11,19,22,26]. In step 3, the battery is discharged with this high potential, capturing the  $M^+$  ions and  $A^-$  from the concentrated solution, interspersing these ions within the crystalline structure of both electrodes at a constant current and in a closed circuit, generating energy. Finally, in step 4, the concentrated solution is exchanged for a recovery solution with low ionic force, leaving the device ready to start a new cycle. During steps 2 and 4, there is no power consumption or generation. Energy extraction,  $W$ , is given by the following expression:

$$W = \oint \Delta E dq = \int_1^2 \Delta E \cdot I \cdot dt + \int_3^4 \Delta E \cdot I \cdot dt \quad (23)$$

where  $I$  is the applied current,  $q$  is the charge, and  $t$  is the time. During the ion capture and release stage, energy extraction ( $W$ ) is given by the sum of thermodynamic and kinetic contributions according the following expression:

$$W = \int_1^2 \Delta E_{eq} \cdot I \cdot dt + \int_3^4 \Delta E_{eq} \cdot I \cdot dt + \int_1^2 \eta \cdot I \cdot dt + \int_3^4 \eta \cdot I \cdot dt = W_{th} + W_k \quad (24)$$

where  $\Delta E_{eq}$  is the equilibrium potential of the electrochemical system,  $\eta$  is the overpotential of the device, and  $W_{th}$  and  $W_k$  are the energy consumption products of the thermodynamic and kinetic contribution, respectively. Kinetic effects are usually related to overpotentials and are essential in determining the amount of energy extracted, on the other hand, kinetic limitations come hand in hand with mass diffusion processes.

### 3. Energy Consumption in the Process of Mixing Entropy Battery (MEB)

The different electrode arrays designs for MEB that have been proposed and successfully applied can be classified as selective exchange and salt capturing methods. The selective exchange is based on an ion intercalation reaction in Prussian Blue Analogue (PBA) while the salt capturing is based on conversion of  $Ag$  to  $AgCl$  [27]. In accordance with Equation (14) the salt capturing method operates using  $FePO_4$  and  $Ag$  as electrodes interacting with  $Li^+$  and  $Cl^-$ , respectively. The selective exchange method operates with one selective electrode  $[Fe^{2+}(CN)_6]$  capable of capturing only metal cations different than  $Li^+$ , in agreement with the following reaction:



The thermodynamic contribution to the energy consumption ( $W_{th}$ ), depends on the method used for the metal ion recovery from the solution. In particular, the equilibrium voltage during step 1 and step 3, according to Figure 1, and the methods are given by the following Nernst equations.

#### 3.1. Thermodynamic Energy Consumption

The thermodynamic energy consumption ( $W_{th}$ ), depends on the method used for the metal recovery, in this case salt capturing and selective exchange methods.

### 3.1.1. Salt Capturing Method

For the salt capturing method, the equilibrium voltage during charge and discharge steps is given by the following Nernst equations, which describe the equilibrium condition of the reaction (14).

$$\Delta E_{eq}(q) = \Delta E^0(q) + \frac{RT}{F} \ln \left[ \frac{q - q_{max}}{F \cdot V_1} \left( c_{Cl,1} + \frac{q - q_{max}}{F \cdot V_1} \right) \right] \quad (26)$$

$$\Delta E_{eq}(q) = \Delta E^0(q) + \frac{RT}{F} \ln [c_{Li,3} \cdot c_{Cl,3}] \quad (27)$$

The thermodynamic energy consumption per mole of  $Li^+$  transferred from the brine to the recovery solution, using the salt capturing method, can be calculated by integrating  $\Delta E_{eq}(q)$  along steps 1 and 3:

$$\frac{W_{th}}{n} = RT \cdot \ln \left[ \frac{n \cdot (V_1 \cdot c_{Cl,1} + n)}{(V_1 \cdot c_{Li,3})(V_1 \cdot c_{Cl,3})} \right] + RT \cdot \frac{V_1 \cdot c_{Cl,1}}{n} \cdot \ln \left[ 1 + \frac{n}{V_1 \cdot c_{Cl,1}} \right] \quad (28)$$

where,  $c$  is concentration and  $V$  is volume of the solution.

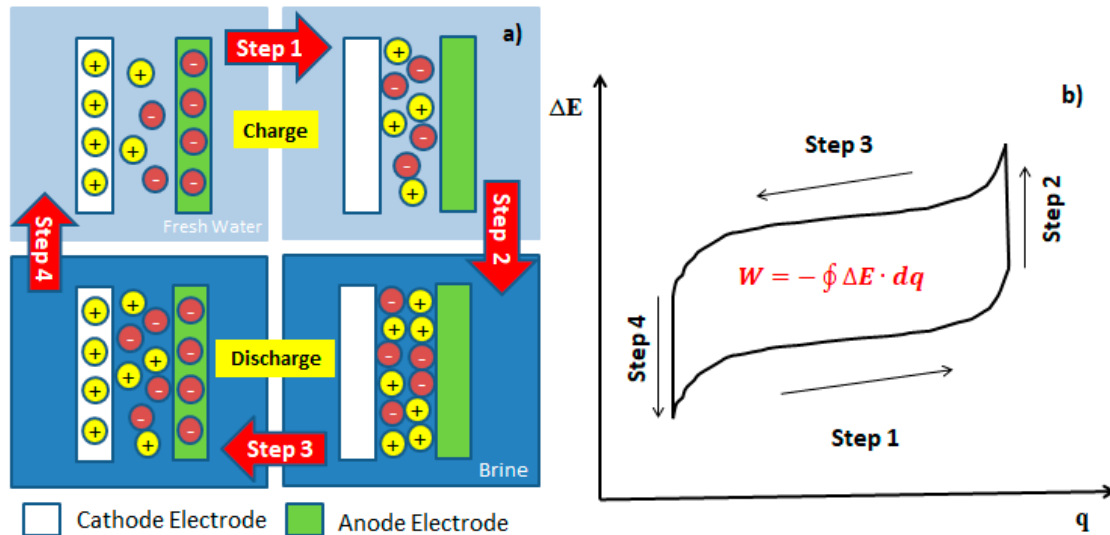


**Figure 1.** (a) Schematic representation of the systematic work of the mixing entropy battery (MEB). (b) Typical Brogioli cycle, where the battery cell voltage ( $\Delta E$ ) vs charge ( $q$ ) is represented. The closed integral represents the removable energy ( $W$ ) of cycle.

### 3.1.2. Selective Exchange Method

In the case of the selective exchange method the equilibrium voltage during charge and discharge steps is given by the following Nernst equations, which describe the equilibrium condition of the reaction (25).

$$\Delta E_{eq}(q) = \Delta E^0(q) + \frac{RT}{F} \ln \left[ \frac{\frac{q - q_{max}}{F \cdot V_1}}{c_{M,1} - \frac{q - q_{max}}{F \cdot V_1}} \right] \quad (29)$$

$$\Delta E_{eq}(q) = \Delta E^0(q) + \frac{RT}{F} \ln \left[ \frac{c_{Li,3}}{c_{M,3}} \right] \quad (30)$$

The subscript  $M$  refers to the metal cation. The thermodynamic energy consumption per mole of  $Li^+$  transferred from the brine to the recovery solution,  $n$ , using the selective exchange method is:

$$\frac{W_{th}}{n} = -RT \cdot \ln \left[ \left( \frac{V_1 c_{M,1}}{n} - 1 \right) \cdot \frac{c_{Li,3}}{c_{M,3}} \right] + RT \cdot \frac{V_1 \cdot c_{M,1}}{n} \cdot \ln \left[ 1 + \frac{n}{V_1 \cdot c_{M,1}} \right] \quad (31)$$

where  $q$  indicates the charge stored in the active material,  $q_{max}$  is the maximum charge stored in the active materials during step 1 and  $\Delta E^0(q)$  is the formal potential of the reaction, which is dependent on the state of charge. The concentration of ions can be considered constant during step 1 and during step 3. The concentration of the ions can change significantly.

### 3.2. Kinetic Energy Consumption

The kinetic energy consumption ( $W_k$ ), is correlated to the overvoltage in the electrochemical device,  $\eta$ . The overvoltage can be divided in three contributions, according to the following equation:

$$\eta = \eta_{el} + \eta_S + \eta_C \quad (32)$$

where  $\eta_{el}$  is the potential drop in the electrolyte,  $\eta_S$  is the overvoltage product charge transfer and  $\eta_C$  is the overpotential product mass transfer. These overpotentials depend on the materials, species involved in the reaction, electrolyte solution and the electrodes materials.

The  $\eta_{el}$  depends on the geometry of the electrochemical device, as well as on the concentration and nature of the ions present in the solution. During step 1 the concentration of the ions in solution does not change significantly, so that the potential drop in the electrolyte can be described by the following equations:

#### 3.2.1. Salt Capturing Method

For the salt capturing method, the drop potential in the electrolyte ( $\eta_{el}$ ) related to the reaction (14) is given by the following equations.

$$\eta_{el} = \frac{\rho_3 \cdot d_3}{A} \cdot I \quad (33)$$

$$\eta_{el} = \frac{V_1 \cdot c_{Cl,1}}{V_1 c_{Cl,1} + \left(\frac{q - q_{max}}{F}\right)} \frac{\rho_1 \cdot d_1}{A} \cdot I \quad (34)$$

#### 3.2.2. Selective Exchange Method

For the selective exchange method, the drop potential in the electrolyte ( $\eta_{el}$ ) related to the reaction the reaction (25) is given by the following equations.

$$\eta_{el} = \frac{\rho_1 \cdot d_1}{A} \cdot I \quad (35)$$

where  $\rho_1$  is the initial resistivity of the recovery solution at the beginning of step 1,  $\rho_3$  is the resistivity of the solution during step 3 and,  $d_1$  and  $d_3$  are the distance between electrodes and  $A$  is the surface area of the electrode. It is assumed that the electrodes are two parallel plate of the same dimensions and that all the cations have similar mobility,  $u_i$ .

$\eta_S$  also is known as the surface overvoltage for both electrodes. In step 3 this overpotential is independent of the electrochemical method. This condition changes only for the salt capturing method in step 1, because of the continuous change in the concentration of the ions in the recovery solution.

The  $\eta_C$  is caused by the transport of reacting and produced species during the electrochemical reaction and strongly depends on the electrochemical method used. In the case of the salt capturing and selective exchange method, the concentration overvoltage during steps 1 and 3 is given by the following:

#### 3.2.3. Salt Capturing Method

For the salt capturing method, the concentration overvoltage for reactants and products ( $\eta_C$ ) related to the reaction (14) is given by the following equations.

$$\eta_C = \frac{RT}{F} \ln \left( 1 + \frac{I \cdot \delta}{A \cdot F \cdot D_{Li} \cdot \left( \frac{q - q_{max}}{F \cdot V_1} \right)} \right) + \frac{RT}{F} \ln \left( 1 + \frac{I \cdot \delta}{A \cdot F \cdot D_{Cl} \cdot \left( c_{Cl,1} + \frac{q - q_{max}}{F \cdot V_1} \right)} \right) \quad (36)$$

$$\eta_C = \frac{RT}{F} \ln \left( 1 + \frac{I \cdot \delta}{A \cdot F \cdot D_{Li} \cdot c_{Li,3}} \right) + \frac{RT}{F} \ln \left( 1 + \frac{I \cdot \delta}{A \cdot F \cdot D_{Cl} \cdot c_{Cl,3}} \right) \quad (37)$$

### 3.2.4. Selective Exchange Method

For the selective exchange method, the concentration overvoltage for reactants and products ( $\eta_C$ ) related to the reaction (25) is given by the following equations.

$$\eta_C = \frac{RT}{F} \ln \left( 1 + \frac{I \cdot \delta}{A \cdot F \cdot D_{Li} \cdot \left( \frac{q - q_{max}}{F \cdot V_1} \right)} \right) - \frac{RT}{F} \ln \left( 1 - \frac{I \cdot \delta}{A \cdot F \cdot D_{Cl} \cdot \left( c_{M,1} - \frac{q - q_{max}}{F \cdot V_1} \right)} \right) \quad (38)$$

$$\eta_C = \frac{RT}{F} \ln \left( 1 + \frac{I \cdot \delta}{A \cdot F \cdot D_{Li} \cdot c_{Li,3}} \right) - \frac{RT}{F} \ln \left( 1 - \frac{I \cdot \delta}{A \cdot F \cdot D_M \cdot c_{M,3}} \right) \quad (39)$$

where  $D_i$  is the diffusion coefficient of species  $i$  and  $\delta$  is the thickness of diffusion layer. Surface overvoltage is strongly dependent on the nature and structure of the active materials used for the recovery of metal cations as  $Li^+$ . It is difficult to predict the value of the surface overvoltage, however it is known that once  $AgCl$  is formed on the surface of  $Ag$  metal,  $\eta_S$  largely increases [5,27,28] and actually represents one of the highest energy losses in the system. Prussian Blue Analogue (PBA) as NiHCF presents a very fast kinetic and very low  $\eta_S$ .

The kinetic energy consumption is always positive and it is observed that the kinetic energy consumption relative to the resistance of the electrolyte and the diffusion process is, in general, small and similar for the two methods when the current density is constant.

## 4. Natural Solutions as Electrolyte for MEB

For the correct MEB operation, it is possible to use the following concentrated electrolytes: seawater, hot-springs water, lake water, underground water, geothermal water, oilfield brine, relict hydrothermal brine, brine from reverse osmosis plants and high-altitude salt-lake brine.

The majority of publications about MEB for harvesting blue energy use a solution of between 0.5 and 0.6 M  $NaCl$  as a concentrated solution (seawater), and 0.02 to 0.024 M  $NaCl$  as a diluted solution (river water) [1,4–6,11,12,19,23]. Seawater is the most abundant electrolyte on Earth; nearly 97.5% of the Earth is covered by seawater, but just 2.5% is fresh water. Obviously, seawater has a significantly higher salt concentration than fresh water due to the existence of salts in the form of dissolved ions at a concentration of about 35 g/L of total salts [29]. On the other hand, the geothermal water composition is characterized by the macro elements of the reservoir rock and the subsurface environment to which it is exposed most of the time. Like seawater, the  $NaCl$  is the most predominant salt component present in dissolved form adding salinity to the geothermal water. The total dissolved solids in high temperature geothermal water (>150 °C) were reported to be between 2.5 to 81 g/L, while for medium temperature geothermal waters it is (90–150 °C). The total dissolved solids were reported to be between 1.1 to 8.2 g/L. The highest concentrations, of between 260 to 280 g/L for geothermal water, have been reported in California, USA [30]. Another interesting alternative is the use of brines from shallow saline lakes or evaporation ponds located in the high altitude plateau of the Salar de Atacama basin in Chile. The total dissolved solid in these brines, around 165 g/L, contains  $Mg^{2+}$ ,  $Ca^{2+}$ ,  $Na^+$ ,  $K^+$ ,  $SO_4^{2-}$ ,  $Cl^-$  and  $HCO_3^-$  as major constituents and also  $B^+$ ,  $Li^+$  and  $Cu^{2+}$  as trace elements. Nevertheless, other elements as  $Co$ ,  $Cr$ ,  $Fe$ ,  $Mn$ ,  $Mo$ ,  $Pb$ ,  $V$ , and  $Zn$ —although confirmed—are not well documented [31]. Table 1, shows the composition of major constituents of different natural brines that have a potential use in this technology.

**Table 1.** Main ion compositions of natural brines.

Ref.	Natural Source	Cl <sup>-</sup> [ppm]	Na <sup>+</sup> [ppm]	Mg <sup>2+</sup> [ppm]	Ca <sup>2+</sup> [ppm]	Li <sup>+</sup> [ppm]
[29,32]	Seawater	19.345	10.752	1.195	0.416	0.179
[33,34]	Geothermal	7.899	4.459	1.700	250	34.27
[35]	Atacama Brine	198.000	42.700	40.500	368	1.820

The main technical limitation of this technology is the fresh water availability. Most publications indicate the use of river water as dilute salt solution. An alternative for fresh water is the use of urban wastewater, which was reported by Meng Ye et al. [22], but no indication was given for the water quality.

## 5. Intercalation Materials as Cathode Electrode in MEB

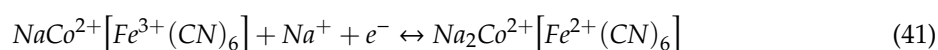
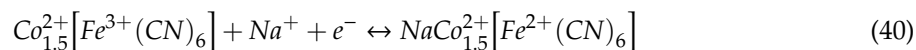
The behavior of a battery is based on the redox reactions which take place on the surface of the electrodes. The equilibrium potential of these reactions depends on the concentration of the electroactive components in the electrolyte solution, which ideally follows a Nernstian response, so that the change of the solution leads to the voltage rise that can be exploited for the energy extraction [1].

Valid candidates to replace the “sodium-capturing electrode” have been found in the PBA family. These materials have an open crystal structure composed of a face-centered cubic setting of transition metal cations octahedrally coordinated to hexacyanometallate groups. Large interstitial “A sites” within the structure can accommodate zeolitic water or alkali insertion ions. This results in a general chemical formula of  $A_xP[R(CN)_6]_{1-y} \cdot y \cdot nH_2O$ , where A is an alkali cation, P is the N-coordinated transition metal cation,  $R(CN)_6$  is the hexacyanometallate anion and represents a hexacyanometallate vacancy. Both the N-coordinated and C-coordinated transition metals can be electrochemically active in this structure. The PBA framework structure has wide channels between the A sites, allowing for the rapid insertion and removal of monovalent and multivalent cations. Some researches verify intercalation of  $Na^+$ ,  $Li^+$ ,  $Mg^{2+}$ ,  $Cu^{2+}$ ,  $Al^{3+}$  and  $NH_4^+$  in PBA [7,8,36–38].

The principal cathode materials, based on PBAs tested in the MEB, are Cobalt Hexacyanoferrate (CoHCF) [23], Nickel Hexacyanoferrate (NiHCF) [27,39] and Copper Hexacyanoferrate (CuHCF) [7,8,11,13,18] to capture  $Na^+$  ions from seawater. The use of materials in the PBA family in MEBs is an advantage, because most are low-cost cathode materials [40].

### 5.1. Cobalt Hexacyanoferrate (CoHCF)

Cobalt Hexacyanoferrate is one of the most interesting inorganic polymers. As shown in Figure 2, the redox process in CoHCF involves two different metal transition ions (Fe and Co). Unlike other materials of the same class, the redox process is driven by a metal to metal charge transfer mechanism. The  $Fe^{3+}$  and  $Co^{3+}$  makes it possible to observe both redox couples,  $Fe^{3+}/Fe^{2+}$  and  $Co^{3+}/Co^{2+}$  in the same material [41]. The principal intercalation reaction for  $Na^+$  ions is shown in the following reactions [23].



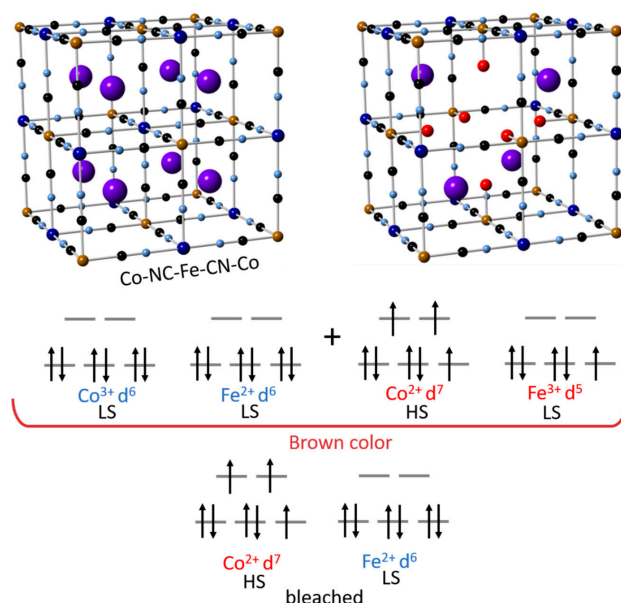


**Figure 2.** Schematic view of the CoHCF crystal structure and expected valence/spin states for the respective redox state (ICSD no. 157486). Illustration based from [42,43].

### 5.2. Nickel Hexacyanoferrate (NiHCF)

Nickel hexacyanoferrate consists of Fe and Ni ions connected by CN- bridges, generating a face-centered cubic structure. In this coordination compound,  $Ni^{2+}$  ions are located in crystal lattice sites occupied by high spin  $Fe^{3+}$  species in PBA. Each Fe ion coordinates with six carbon atoms, whilst each Ni ion coordinates with six nitrogen atoms. This arrangement produces an open-channel network along the three crystallographic axes, which allows for electroinsertion/electrodeinsertion of hydrated cations [27,39,44], as shown in Figure 3.

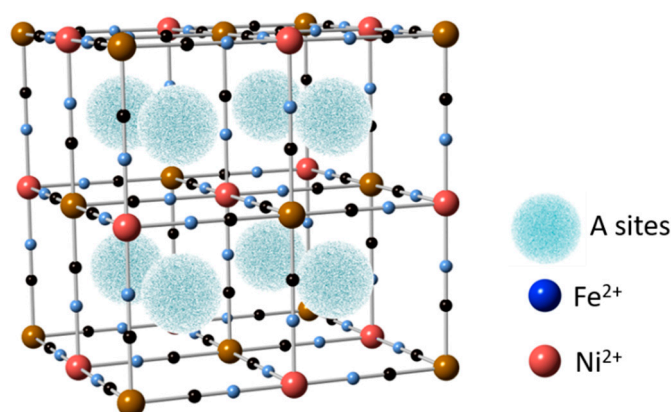
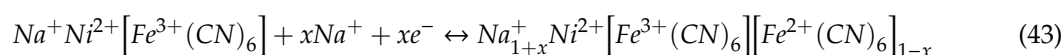
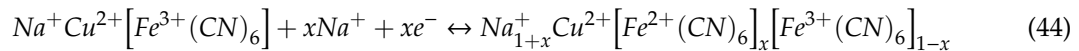


**Figure 3.** Crystal structure of Nickel Hexacyanoferrate (NiHCF) (ICSD no. 89338). Illustration based on [44,45].

### 5.3. Copper Hexacyanoferrate (CuHCF)

This material showed a very good potential for mono and multivalent ions insertion and de-insertion characteristics. The capacity of CuHCF is insensitive to the ionic valency of the intercalating

species provided. The concentration of intercalating ions in the electrolyte is more than the moles of the active material, this is because the number of ions inserted in the CuHCF depends on the balancing of charge with the number of available  $Fe^{2+}$  ions in the crystal structure, thereby limiting the cell capacity [8,13].



The reduction reaction corresponds to the collation process, and oxidation to the deintercalation process of  $Na^+$  ions. When the reduction process occurs, the reduction of  $Fe^{3+}$  ions to  $Fe^{2+}$  occurs simultaneously. At the same time, for the  $Na^+$  ion insertion process to be carried out within the crystalline structure of PBA, a lot of energy or work force will be needed, because in some PBAs the  $K^+$  ions occupy the center of the structure, as shown in Figure 4. During the oxidation process of  $Fe^{2+}$  to  $Fe^{3+}$  the deintercalation of  $Na^+$  ions will simultaneously occur.

Nowadays, PBAs are the cheapest cathode materials used in MEBs [40]. These materials don't need high temperatures for synthesis because the material can be obtained at ambient temperature. Table 2 shows the most typical cathode materials used in MEB, indicated in the bibliography, and their operation conditions.

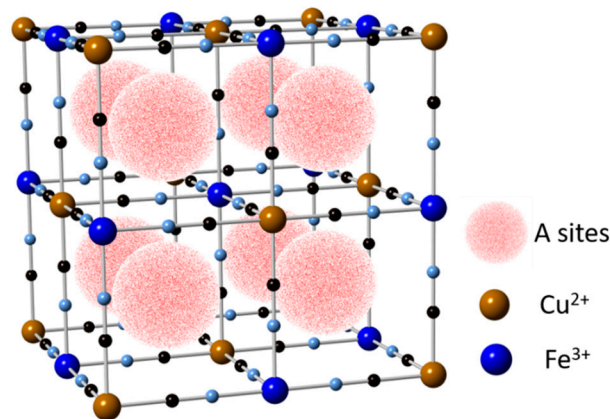


**Figure 4.** Schematic structure of Copper Hexacyanoferrate (CuHCF) (ICSD no. 99499). Illustration based from [36,46].

**Table 2.** Prussia blue analogue material as cathode in MEBs.

Ref.	PBA	Electrode Area [cm <sup>2</sup> ]	Range Potential [V]	Range Density Current [A/cm <sup>2</sup> ]	N <sup>o</sup> Cycle	Gain Voltage [V]
[11]	CuHCF	5	0.2–0.65	±0.1	10	0.102
[7]	CuHCF	7	0–0.8	±0.2	20	0.172
[8]	CuHCF	3	0–0.9	±0.5	-	0.172
[13]	CuHCF	1	-	±0.2	50	-
[23]	CoHCF	1.3	0–1.1	±0.01	30	0.153
[39]	NiHCF	1	0–0.6	±0.01	-	-

#### 5.4. $LiFePO_4$

The topotactic insertion of  $Li^+$  ions into heterosite ( $FePO_4$ ) is used successfully in lithium iron phosphate rechargeable battery. The  $LiFePO_4$  in the olivine phase is more stable than insertion of  $Na^+$ , accepting lithium in preference to other cations on exposure in the aqueous solution. The high mobility of  $Li^+$  in the structure shows the fast discharge reaction, suggesting that  $Li^+$  insertion is controlled by the time of exposure of  $FePO_4$  material to solutions that contain  $Li^+$ , indicated by the fast kinetic. The insertion of  $Na^+$  into heterosite  $FePO_4$  involves a large volumetric expansion,

structural rearrangement, and low kinetics and the presence of a small amount of  $Li^+$  ions. The  $FePO_4$  matrix seems to block the insertion of  $Na^+$  [5,47,48], as shown in Figure 5.

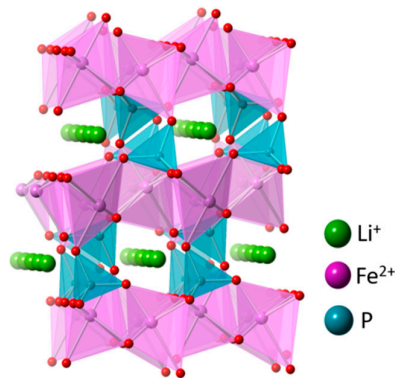
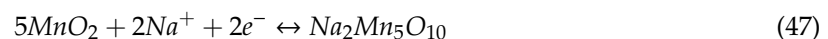


**Figure 5.** Crystal structure of olivine  $LiFePO_4$  in projection [001] (ICSD no. 56291).

### 5.5. $Na_2Mn_5O_{10}$

Manganese dioxide-based materials are used as supercapacitor and are studied for their good electrochemical behavior, high specific capacitance, environmental-friendliness and low cost. Among the large quantities of manganese oxides reported in literature are Li-Mn-O, Na-Mn-O or Mg-Mn-O systems, which received extensive attention due to their tunnel or layered crystal structures, facilitating the cation intercalation/deintercalation [49] as shown in Figure 6. A  $Mn^{4+}/Mn^{3+}$  redox system involving a single-electron transfer is responsible for the  $MnO_2$  pseudocapacitive behavior. The energy storage mechanism is generally related to the accumulation of ionic charges in the double layer at the electrode/electrolyte interface. In aqueous electrolytes the charge/discharge is described by the following equation [5,50]:



where  $M^+$  represents metal cations as  $Na^+$ ,  $Li^+$  and  $K^+$ . The reaction mechanism implies an adsorption/desorption process of cations at the material surface and/or an insertion/extraction process of cations into the bulk material. The charge storage consists of a complete reduction of  $Mn^{4+}/Mn^{3+}$  energy extracted from  $MnO_2$ , depending strongly on the quality of the material collector interface of the supercapacitor [50].

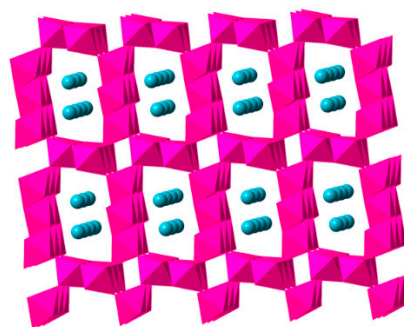


**Figure 6.** Schematic illustration of the crystal structure of  $Na_2Mn_5O_{10}$ . This structure consists of purple octahedral units  $MnO_6$  shared by corners and/or edges, where  $Na^+$  occupies positions within channels formed by octahedrals units (JCPDS 27-0749).

### 5.6. $\text{Na}_4\text{Mn}_9\text{O}_{18}$

The sodium manganese oxide has been considered as a promising cathode material in the  $\text{Na}^+$  ion battery. The orthorhombic structure of sodium manganese oxides is dependent on the sodium content, and it is made of  $\text{MnO}_5$  square pyramids and  $\text{MnO}_6$  octahedral as shown in Figure 7. The manganese ions are located in two different environments, leading to three available sites in which two  $\text{Na}^+$  ions occupy the large s-shaped tunnels while another  $\text{Na}^+$  ion occupies a smaller tunnel [51], according to the follow equation [22]:



Table 3 shows the most typical battery materials and the principal parameters used in the MEB for operation and design of the electrochemical device. These parameters deliver the constructive form of the MEB. The volume of the test battery indicates that the technology is of laboratory scale and has not yet been tested on a pilot scale. All MEB use parallel plate electrodes in their design, and the electrode distance is also important because the internal resistance of electrolytes is reduced by decreasing the distance between electrodes [22].

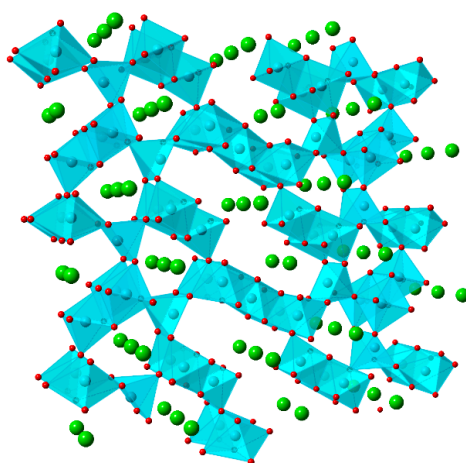


**Figure 7.** Schematic illustration of the crystal structure of  $\text{Na}_4\text{Mn}_9\text{O}_{18}$ . The Mn atoms form alternated octahedron  $\text{MnO}_6$  and tetrahedron  $\text{MnO}_4$  to form a several channels where diffusion of  $\text{Li}^+$  ions occurs (MP-1094147).

**Table 3.** Battery materials used as cathodes in MEBs.

Ref.	BM	Electrode Area [ $\text{cm}^2$ ]	Volume MEB [ $\text{cm}^3$ ]	Range Potential [V]	Electrode Distance [mm]	Range Density Current [ $\text{A}/\text{cm}^2$ ]	N° Cycle
[5]	$\text{LiFePO}_4$	2	0.35	0–0.5	10	$\pm 0.5$	100
[5]	$\text{Na}_2\text{Mn}_5\text{O}_{10}$	2	0.35	-	10	$\pm 0.25$	100
[1]	$\text{Na}_2\text{Mn}_5\text{O}_{10}$	1	-	-	0.6	-	-
[22]	$\text{Na}_4\text{Mn}_9\text{O}_{18}$	9	1.5	-	1.7	$\pm 0.03$	12
[3]	$\text{Na}_4\text{Mn}_9\text{O}_{18}$	3.01	0.06	0–0.6	0.2	$\pm 0.5$	3

Table 4 shows information about the suspension preparation procedure for the active material in the cathode electrodes. The active material is mixed with a polyvinylidene fluoride (PVDF) as a binder, carbon black or graphite and N-Methyl-2-pyrrolidone (NMP), 1-Methyl-2-pyrrolidinone or dimethyl sulfoxide as solvent.

**Table 4.** Preparation of battery material and PBA for cathodes in MEBs.

Ref.	Active Material	Synthesis Method	Covering Method	Active Material [%]	Substrate	Electrode Mass [mg/cm <sup>2</sup> ]
[5]	LiFePO <sub>4</sub>	Polymeric Synthesis	Drop Casting	80	Carbon Cloth	25
[22]	Na <sub>4</sub> Mn <sub>9</sub> O <sub>18</sub>	Solid State Reaction	Ink Coating	85	Carbon Cloth	14
[1]	Na <sub>2</sub> Mn <sub>5</sub> O <sub>10</sub>	Pachini Method	Doctor Blade	80	Graphite	8
[7]	MnO <sub>2</sub>	Co-Precipitation	Doctor Blade	70	Graphite Sheet	34
[11]	CuHCF	Dropwise	Spread	90	Carbon Plate	5
[7]	CuHCF	Co-Precipitation	Doctor Blade	70	Graphite Sheet	-
[8]	CuHCF	Co-Precipitation	Doctor Blade	70	Graphite Foil	4.4
[13]	CuHCF	Co-Precipitation	Spread	80	Carbon Paper	4.8
[23]	CoHCF	Co-Precipitation	Electrodeposition	-	CPE	0.193
[39]	NiHCF	Co-Precipitation	Hand Painting	80	Carbon Cloth	-

Table 5 shows information regarding the blue energy recovery obtained by various researchers using different active materials for the MEB.

**Table 5.** Blue energy recovery using different cathode materials.

Ref.	Active Material	Relevant Characteristics		Reversible Capacity [mAh/g]	Efficiency [%]	Blue Energy Recovery
		Advantage	Disadvantage			
[5]	LiFePO <sub>4</sub>	High Stability	Poor E.C	120	-	13.5 μW/cm <sup>2</sup>
[22]	Na <sub>4</sub> Mn <sub>9</sub> O <sub>18</sub>	High Capacity Retention	Low Charge Capacity	113	68	0.65 kW/m <sup>3</sup>
[5]	Na <sub>2</sub> Mn <sub>5</sub> O <sub>10</sub>	High Surface Area	Low Charge Capacity	-	75	10.5 μW/cm <sup>2</sup>
[11]	CuHCF			-	69	13990 μW/cm <sup>2</sup>
[7]	CuHCF	High Capacity	High Irreversible Reaction	-	-	411 mW/m <sup>2</sup>
[8]	CuHCF			-	-	6.3 mW/m <sup>2</sup>
[13]	CuHCF			-	-	87 mW/m <sup>2</sup>
[23]	CoHCF	High Energy Density	Cell Voltage Limited (<1 V)	130	65	4632 μW/cm <sup>2</sup>
[39]	NiHCF	Efficient Energy Consumption	Low water recovery	60	-	16.8 kJ/mol

Many groups are focusing on a synthesis of new material electrodes with high specific capacity and cycling steadiness. Also, efforts have been directed to simplify electrode manufacturing processes. The most commonly used electrode materials have been modified by elemental doping, coating and composting with other materials like LiNiMnCoO<sub>2</sub> [52]. These imply high ion diffusivity, enhancement in conductivity, ionic mobility and high retention capacity during the charging/discharging process. According to the reaction mechanisms of electrode materials, the materials can be divided into two groups, namely insertion and conversion type materials [53]. The literature shows that insertion materials are more promising materials because a robust crystalline structure, enlarged diffusion channel and easier pathways for ion insertion and removal are achieved. These provide a long-term cycling stability and high rate capability in comparison with conversion electrodes like *Ag* or *Bi*. These characteristics imply excellent stability and good safety performance for the intercalation material, and therefore are a preferred choice in commercial batteries [54].

## 6. Anode Materials Used in MEB

The anode materials used in MEB devices must have a very good redox behavior in contact with Cl<sup>-</sup> ions, as the intercalation or reaction of the electrodes with Cl<sup>-</sup> will result in energy storage. The silver electrode is a precious metal that reacts with Cl<sup>-</sup> to produce AgCl in addition to side complexation reactions, not only with chloride but also with sulfate in seawater. Searching alternative anode electrodes is essential for the development of MEBs.

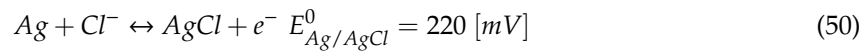
### 6.1. Silver

Silver (Ag) electrodes are the most popular anodic electrodes [13] used in MEBs because of their reversibility and adaptability features in the presence of Cl<sup>-</sup> ions. The reason is that the anodic AgCl phase formation can take in an electrochemical window devoid of oxygen evolution reaction [55].

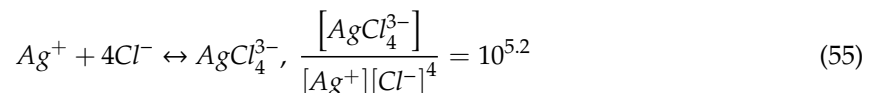
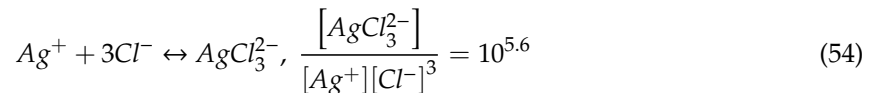
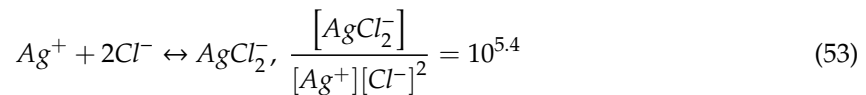
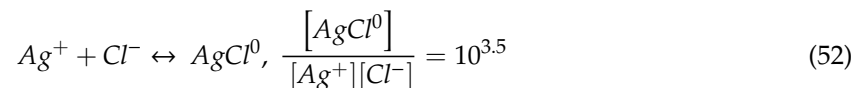
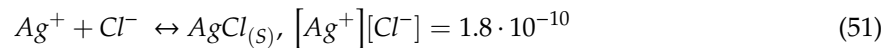
Unfortunately,  $AgCl$  phase formation takes place through many different forms of parallel reactions, as follows:



The typical anodic reactions  $n = 1$  ( $n = 1,2,3$ ) with thermodynamic stabilities [56] take place according to the following equations [5,22,27,28,54–56]:

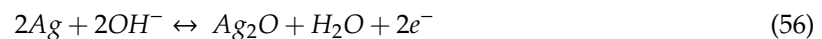


The most relevant reactions and their equilibrium constants are [22]



The equilibrium concentration of the total soluble  $Ag^+$  is about 8.9 ppm, almost 100 times the U.S EPA secondary drinking water standard of 0.1 ppm.  $Ag^+$  is known to cause adverse health effects, including argyria, argyrosis, liver and kidney damage [22]. At present, the behavior of  $Ag$  in hypersaline solutions such as Atacama brines has not yet been studied.

Over 500 mV, the anodic current increases, due to the occurrence of reactions with the  $OH^-$  ion at pH 7 or close to neutral, according to the following equation [57,58]:



$AgCl$  formation mechanisms on the  $Ag$  surface electrode have been identified as a two-dimensional monolayer that is formed in the first adsorption/desorption cycle. After that, the  $AgCl$  phase or thin film grows by nucleation on the first layer as shown in Figure 8. During the formation of  $AgCl$  film over the  $Ag$  substrate, the overpotential gradually increases due to the resistance of deposit film. The overpotential fluctuation has been attributed to the cracking and healing of the  $AgCl$  layer or the dissolution of  $AgCl$  deposit accompanying the deposit growth [60–62].

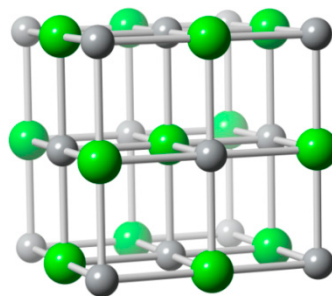


**Figure 8.** The  $AgCl$  structure, a FCC unit cell with two ions (ICSD no. 56538) ( $Ag$  and  $Cl^-$  are gray and green atoms respectively) per lattice point.

### 6.2. Bismuth Oxychloride (BiOCl)

In 2019 G. Tan et al. [13] presented Bismuth Oxychloride (*BiOCl*) as an alternative to the *Ag* metal as anode. *BiOCl* has a tetragonal structure as shown in Figure 9 and is composed of a layer of  $Cl^-$ ,  $Bi^{3+}$  and  $O^{2-}$  ions, and was successfully employed in chloride ion batteries and faradic deionization systems as chloride ( $Cl^-$ ) release/capture electrodes. *BiOCl* showed two kinds of reversible reactions due to  $Cl^-$  transfer during cycling: (i) a major conversion reaction in which *BiOCl* transformed to *Bi* metal and  $Bi_2O_3$ , and (ii) a minor intercalation process that *BiOCl* charged to  $BiOCl_{1-x}$  ( $x > 0$ ) [61]. The principal reaction that occurs during charge and a discharge step is:



### 6.3. Polypyrrole (PPy)

This compound is another promising material successfully tested as anode electrode [39,62,63]. The *PPy* material as an organic conducting polymer has been implemented with pyrrole-based polymers in which anionic dopants are incorporated upon preparation of the anode electrode as shown in Figure 10. The *PPy* is insoluble in aqueous electrolytes [63] and due to its wide potential window, complemented with high electron conductivity and good mechanical properties, has a wide potential range of technological applications [64]. The following mechanism of anion doping occurs by means of the following expression:

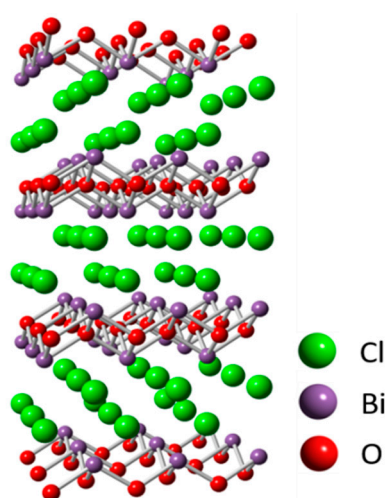
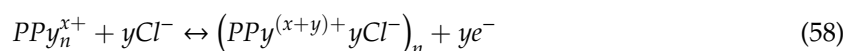
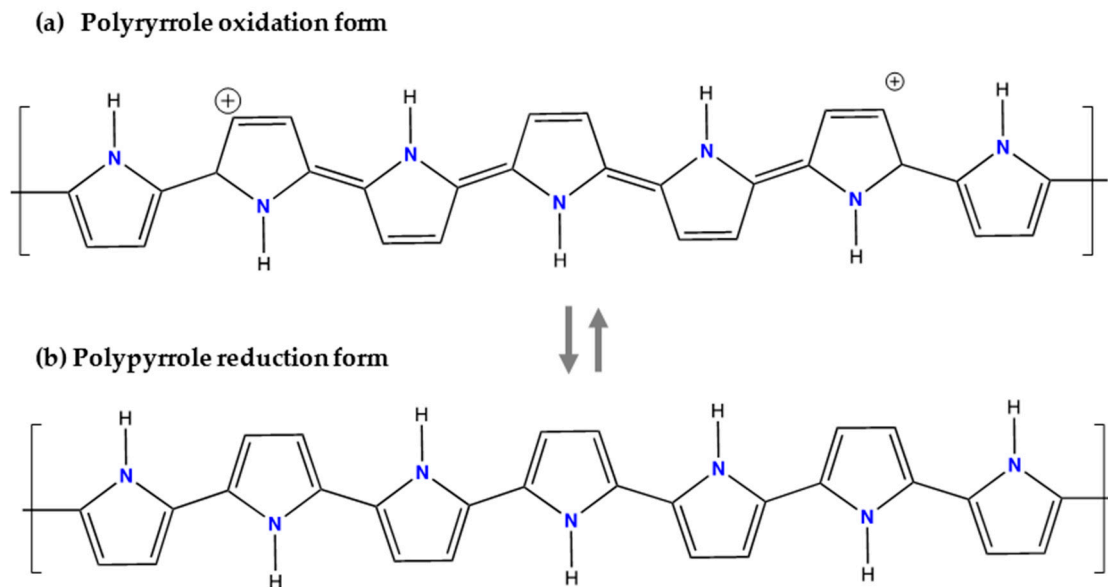


Figure 9. Schematic 2D layer structure of BiOCl (ICSD no. 74502).

The conductivity of these conjugated polymers can be enhanced by oxidation of their chains. Oxidation/reduction processes also known as doping/de-doping are commonly accompanied by an ion flow in the electrode/solution interface, which maintains the electroneutrality of the polymer matrix [64]. The first step is the coordination of the anions from the electrolyte with the *PPy* chains during oxidation, which are then released during reduction. The reaction potentially of *PPy* depends on the particular doping anion. The *Ag/PPy* electrode consists of silver particles dispersed in *PPy* and was used in a MEB by Gomes et al. [39].



**Figure 10.** Structure of Polypyrrole for respective redox states. Illustration based from [65].

The Table 6 shows the anode materials that used until now in MEB technology. The difference between them is the energy consumption in the process of capturing the  $Cl^-$ . Under similar conditions, the  $AgCl$  and  $BiOCl$  needed much more energy than  $PPy$  without considering that  $Ag$  has a higher cost than  $Bi$  and  $PPy$ . The costs are 3 USD/kg, 9.8 USD/kg and 553 USD/kg for  $PPy$ ,  $Bi$  and  $Ag$  respectively [40,66].

**Table 6.** Anode material used in MEB.

Ref.	Anode Material	Covering Method	Material [%]	Substrate	Electrode Mass [mg/cm <sup>2</sup> ]
[5]	Ag	Drop Casting	85	Carbon Cloth	40
[22]	Ag	Ink Coating	85	Carbon Cloth	10
[1]	Ag	Ag Foil	100	-	-
[23]	Ag	Ag Sheet	100	Cu-CPE	-
[13]	BiOCl	Spread	80	Carbon Paper	4.8
[39]	PPy/Ag	Electropolymerization	-	ITO	-

## 7. Conclusions and Outlooks

Salinity gradient energy or blue energy using MEBs is clearly a plausible alternative to renewable energy around the world. In comparison with classical marine energies based on the mechanical action of waves and coastal wind, the blue energy presents interesting advantages related to reduced installation and material costs and corrosion protection requirements in coastal areas. However the working conditions in coastal areas pose a challenge for an MEB installation to overcome long term exposure to humidity with high salinity, wave action, splash and high corrosive stress, which together give rise to very fast corrosion in important sectors of a plant, increasing, as a result, the cost of this alternative energy harvesting [67]. The latest developments in this area, towards new and more efficient blue energy devices, encourage new ideas for the development of environmentally friendly projects. While blue energy is closely related to the recovery of chemical energy from the mixture of seawater and the river water that flows into the sea, it is also true that it is possible to consider other alternatives, such as the following:

- (a) Synthetic or natural saline solutions such as altiplanic brines in South America can serve as electrolytes in areas where no rivers with considerable flows are available. This alternative opens the possibility for this technology to be used in nearby coastal areas, or high altitude salt lake brines, as is the case for many altiplanic places in South America.

- (b) Another possibility would be to consider rejection flows from reverse osmosis plants as concentrated NaCl solution and seawater as the diluted solution in arid places where there are no rivers or treatment plants that flow into the sea.
- (c) It is interesting to note that fresh water availability, which is the main restrictive factor to implement MEB technologies in arid places, can be overcome by using solar energy to obtain distilled water with complete recycling of the electrolyte to achieve conversion of solar energy into electrical energy. The solar distillation technologies are well known and have a historical record of applications in Northern Chile as far back as 1842 and worked effectively for 40 years [68]. This fresh water collection alternative would make harvesting energy from salinity gradient possible at lower costs and greater efficiency.
- (d) The use of wastewater effluents as a source of fresh water could be useful for obtaining electrical energy through MEBs. However, more research related to the behavior of electrodes in the presence of biological contaminants and free chlorine is needed.

Today the efforts of many researchers are focused on the search for new cathode materials capable of storing the greatest amount of energy with good reversibility as well as low over-potentials and the lowest self-shocks or electrical leaks. This condition enables a good response under high intensity charging and discharging cycles, in addition to lower operational costs that overall fulfill a requirement for an environmentally friendly technology.

The proof-of-concept for MEB studies tested with a combination of different electrolytes such as real wastewater effluent, fresh water or artificial recovery solutions; real or artificial seawater or brine; with Sodium Manganese Oxide (NMO) or Lithium Iron Phosphate (LFP) as a cationic electrode and Ag/AgCl as anionic electrode have been shown to have high energy recovery efficiency values (68 to 75%). Unfortunately, some drawbacks are that (i) the Ag/AgCl electrode is costly and partially soluble in seawater or hypersaline solutions such as Atacama brines, (ii) the NMO and LFP electrodes are also costly with a moderate specific capacity and (iii) the MEB operation requires a charging step with an upfront energy investment, increasing the operational complexity. A very convenient attribute is the open-framework structure belonging to PBA materials, that allows fast insertion/extraction of cations into/from the interstitial sites or crystal structure, evidenced by over 1000 charge/discharge cycles and lower cost (<1 USD/kg) [40].

It is interesting that anionic materials in electrochemical devices such as Bi/BiOCl, Ag/AgCl and PPy have not only been tested in MEB batteries but also in chloride sensors, deionization devices and Lithium recovery from brines. The initial high adsorption/desorption activity for Cl<sup>-</sup> ions exhibited by Ag/AgCl and BiOCl degrades during the cycles, as higher thermodynamic and kinetic energy consumptions gradually increase, whereby the recovered blue energy is reduced over time. The PPy that is the cheapest material (<3 USD/kg) [40] as anode electrode presents the best behavior when capturing Cl<sup>-</sup> ions during cycling, this being manifested as a lower energy consumption. In this potential range the PPy electrode also showed an excellent cycling performance that was close to 100% coulombic efficiency (ranging from 95.7 to 97.8%) and 92% capacity retention through 50 cycles [40].

Other reported electrodes made of inorganic materials such as MgMn<sub>2</sub>O<sub>4</sub> [69–71], Na<sub>2</sub>FeP<sub>2</sub>O<sub>7</sub> [72], NaTi<sub>2</sub>(PO<sub>4</sub>)<sub>3</sub> [73], Na<sub>0.44</sub>MnO<sub>2</sub> [74], FeFe(CN)<sub>6</sub> [75], K<sub>4</sub>Fe(CN)<sub>6</sub> [76], K<sub>0.03</sub>Cu[Fe(CN)<sub>6</sub>]<sub>0.65</sub> · 0.43H<sub>2</sub>O [77], NaFeHCF [78], MnHCF [79], Na<sub>3</sub>V<sub>2</sub>(PO<sub>4</sub>)<sub>3</sub> [80], NaMnO<sub>2</sub> [81] and NaNiHCF [78] have been explored as active materials for Faradaic ions storage in electrochemical desalination devices.

Recently new anode materials have been reported and are under development, such as TiOCl [82], VOCl [83,84], VOCl<sub>2</sub> [83,84], SnOCl<sub>2</sub> [85], FeOCl [86–88], PbCl<sub>2</sub> [89] and Bi<sub>2</sub>O<sub>3</sub> [90].

Thus, at present development of the MEB technology, PBA and PPy seem to be the ideal candidates to be used as cationic and anionic electrode materials. Both have lower costs, overlapping potential range, sensitivity to NaCl and LiCl concentration changes and excellent cycling performance and stability in aqueous solutions.

**Author Contributions:** Conceptualization, methodology, and writing-original draft preparation, F.G.; visualization, writing review and editing, L.C.; sources and editing, L.M.; visualization, writing review and editing, Á.S. All authors have read and agreed to the published version of the manuscript.

**Funding:** This research received no external funding.

**Acknowledgments:** The author would like to the Programa de Doctorado en Ingeniería de Procesos de Minerales of the University of Antofagasta, Chile.

**Conflicts of Interest:** The authors declare no conflict of interest.

## References

1. Marino, M.; Misuri, L.; Ruffo, R.; Brogioli, D. Electrode kinetics in the “capacitive mixing” and “battery mixing” techniques for energy production from salinity differences. *Electrochim. Acta* **2015**, *176*, 1065–1073. [[CrossRef](#)]
2. Marino, M.; Misuri, L.; Carati, A.; Brogioli, D. Proof-of-Concept of a Zinc-Silver Battery for the Extraction of Energy from a Concentration Difference. *Energies* **2014**, *7*, 3664–3683. [[CrossRef](#)]
3. Lee, J.; Yoon, H.; Lee, J.; Kim, T.; Yoon, J. Extraction of Salinity Gradient Energy using a Hybrid Capacitive-mixing System. *ChemSusChem* **2017**, *10*, 1600–1606. [[CrossRef](#)] [[PubMed](#)]
4. Brogioli, D. Extracting renewable energy from a salinity difference using a capacitor. *Phys. Rev. Lett.* **2009**, *058501*, 31–34. [[CrossRef](#)]
5. La Mantia, F.; Pasta, M.; Deshazer, H.D.; Logan, B.E.; Cui, Y. Batteries for Efficient Energy Extraction from a Water Salinity Difference. *Nanoletters* **2011**, *11*, 1810–1813. [[CrossRef](#)]
6. Brogioli, D.; Ziano, R.; Rica, R.A.; Salerno, D.; Kozynchenko, O.; Hamelers, H.V.M.; Mantegazza, F. Exploiting the spontaneous potential of the electrodes used in the capacitive mixing technique for the extraction of energy from salinity difference. *Energy Environ. Sci.* **2012**, *5*, 9870–9880. [[CrossRef](#)]
7. Kim, T.; Rahimi, M.; Logan, B.E.; Gorski, C.A. Evaluating Battery-like Reactions to Harvest Energy from Salinity Differences using Ammonium Bicarbonate Salt Solutions. *ChemSusChem* **2016**, *9*, 981–988. [[CrossRef](#)]
8. Kim, T.; Rahimi, M.; Logan, B.E.; Gorski, C.A. Harvesting energy from salinity differences using battery electrodes in a concentration flow cell. *Environ. Sci. Technol.* **2016**. [[CrossRef](#)]
9. Morais, W.G.; Gomes, W.J.A.S.; Huguenin, F. Neutralization Pseudocapacitors: An Acid-Base Machine. *J. Phys. Chem. C* **2016**, *120*, 17872–17877. [[CrossRef](#)]
10. Hasan, K.N.; Khai, T.X.; Kannan, R.; Zakaria, Z.A. Harnessing Blue energy: A Review Techniques and Preliminary Analysis. *MATEC Web Conf.* **2017**, *131*, 04013. [[CrossRef](#)]
11. Jia, Z.; Wang, B.; Song, S.; Fan, Y. A membrane-less Na ion battery-based CAPMIX cell for energy extraction using water salinity gradients. *RSC* **2013**, *3*, 26205–26209. [[CrossRef](#)]
12. Sharma, K.; Kim, Y.H.; Yiaccoumi, S.; Gabitto, J.; Bilheux, H.Z.; Santodonato, L.J.; Mayes, R.T.; Dai, S.; Tsouris, C. Analysis and simulation of a blue energy cycle. *Renew. Energy* **2016**, *91*, 249–260. [[CrossRef](#)]
13. Tan, G.; Zhu, X. Polyelectrolyte-coated CuHCF and BiOCl electrodes for efficient salinity gradient energy recovery in capacitive mixing. *Energy Technol.* **2019**, *8*. [[CrossRef](#)]
14. Logan, B.E.; Elimelech, M.; States, U. Membrane-based processes for sustainable power generation using water. *Nature* **2012**. [[CrossRef](#)]
15. Sales, B.B.; Liu, F.; Schaeztle, O.; Buisman, C.J.N.; Hamelers, H.V.M. Electrochemical characterization of a supercapacitor flow cell for power production from salinity gradients. *Electrochim. Acta* **2012**, *86*, 298–304. [[CrossRef](#)]
16. Pattle, R.E. Production of Electric Power by Mixing Fresh and Salt Water in the Hydroelectric Pile. *Nature* **1954**, *174*, 660. [[CrossRef](#)]
17. Clampitt, B.H.; Kiviat, F.E. Energy recovery from saline water by means of electrochemical cells. *Sci. New Ser.* **1976**, *194*, 719–720. [[CrossRef](#)]
18. Jia, Z.; Wang, B.; Song, S.; Fan, Y. Blue energy: Current technologies for sustainable power generation from water salinity gradient. *Renew. Sustain. Energy Rev.* **2014**, *31*, 91–100. [[CrossRef](#)]
19. Marino, M.; Kozynchenko, O.; Tennison, S.; Brogioli, D. Capacitive mixing with electrodes of the same kind for energy production from salinity differences. *J. Phys. Condens. Matter* **2016**, *28*, 114004. [[CrossRef](#)]

20. Post, J.W.; Hamelers, H.V.M.; Buisman, C.J.N. Energy Recovery from Controlled Mixing Salt and Fresh Water with a Reverse Electrodialysis System. *Environ. Sci. Technol.* **2008**, *42*, 5785–5790. [[CrossRef](#)]
21. Pasta, M.; Battistel, A.; Mantia, F. La Batteries for lithium recovery from brines. *Energy Environ. Sci.* **2012**, *5*, 9487–9491. [[CrossRef](#)]
22. Ye, M.; Pasta, M.; Xie, X.; Cui, Y.; Criddle, S. Performance of a Mixing Entropy Battery Alternately Flushed with Wastewater Effluent and Seawater for Recovery of Salinity-gradient Energy - Supplementary Information. *Energy Environ. Sci.* **2014**, 1–8.
23. Tehrani, S.H.M.H.; Seyedsadjadi, S.A.; Ghaffarinejad, A. Application of electrodeposited cobalt hexacyanoferrate film to extract energy from water salinity gradients. *RSC Adv.* **2015**, *5*, 30032–30037. [[CrossRef](#)]
24. Nie, P.; Yuan, J.; Wang, J.; Le, Z.; Xu, G.; Hao, L.; Pang, G.; Wu, Y.; Yan, X.; Zhang, X. Prussian Blue Analogue with Fast Kinetics Through Electronic Coupling for Sodium Ion Batteries. *Appl. Mater. Interfaces* **2017**, *9*, 20306–20312. [[CrossRef](#)] [[PubMed](#)]
25. Liao, J.; Hu, Q.; Yu, Y.; Wang, H.; Tang, Z.; Wen, Z.; Chen, C. Potassium-rich iron hexacyanoferrate/dipotassium terephthalate @carbon nanotube composite for K-ion full cells with optimized electrolyte. *J. Mater. Chem. A* **2017**, *0*, 19017–19024. [[CrossRef](#)]
26. Rica, R.A.; Ziano, R.; Salerno, D.; Mantegazza, F.; van Roij, R.; Brogioli, D. Capacitive Mixing for Harvesting the Free Energy of Solutions at Different Concentrations. *Entropy* **2013**, *15*, 1388–1407. [[CrossRef](#)]
27. Trocoli, R.; Bidhendi, G.K.; Mantia, F. La Lithium recovery by means of electrochemical ion pumping: A comparison between salt capturing and selective exchange. *J. Phys. Condens. Matter* **2016**, *28*, 114005. [[CrossRef](#)]
28. Pasta, M.; Wessells, C.D.; Cui, Y.; La Mantia, F. A Desalination Battery. *Nanoletters* **2012**, *12*, 839–843. [[CrossRef](#)]
29. Senthilkumar, S.T.; Go, W.; Han, J.; Thuy, L.P.T.; Kishor, K.; Kim, Y.; Kim, Y. Emergence of rechargeable seawater batteries. *J. Mater. Chem. A* **2019**, *7*, 22803–22825. [[CrossRef](#)]
30. Gude, G. *Geothermal Source for Water Desalination—Challenges and Opportunities*; Butterworth-Heinemann: Oxford, UK, 2018; Volume 1, ISBN 9780128152447.
31. Tapia, J.; González, R.; Townley, B.; Oliveros, V.; Álvarez, F.; Aguilar, G.; Menzies, A.; Calderón, M. Geology and geochemistry of the Atacama Desert. *Antonie van Leeuwenhoek Int. J. Gen. Mol. Microbiol.* **2018**, *111*, 1273–1291. [[CrossRef](#)]
32. Bardi, U. Extracting Minerals from Seawater: An Energy Analysis. *Sustainability* **2010**, *2*, 980–992. [[CrossRef](#)]
33. Cortecchi, G.; Boschetti, T.; Mussi, M.; Lameli, C.H.; Mucchino, C.; Barbieri, M. New chemical and original isotopic data on waters from El Tatio geothermal field, northern Chile. *Geochem. J.* **2005**, *39*, 547–571. [[CrossRef](#)]
34. Taylor, P.; Park, J.; Sato, H.; Nishihama, S. Solvent Extraction and Ion Exchange Lithium Recovery from Geothermal Water by Combined Adsorption Methods. *Solvent Extr. Ion Exch.* **2012**, *30*, 398–404. [[CrossRef](#)]
35. Ogawa, Y.; Koibuchi, H.; Suto, K.; Inoue, C. Effects of the Chemical Compositions of Salars de Uyuni and Atacama Brines on Lithium Concentration during Evaporation. *Resour. Geol.* **2014**, *64*, 91–101. [[CrossRef](#)]
36. Guduru, R.K.; Icaza, J.C. A Brief Review on Multivalent Intercalation Batteries with Aqueous Electrolytes. *Nanomaterials* **2016**, *6*, 41. [[CrossRef](#)]
37. Yang, N.; Sun, H. Biocoordination chemistry of bismuth: Recent advances. *Coord. Chem. Rev.* **2007**, *251*, 2354–2366. [[CrossRef](#)]
38. Ma, F.; Li, Q.; Wang, T.; Zhang, H.; Wu, G. Energy storage materials derived from Prussian blue analogues. *Sci. Bull.* **2017**, *62*, 358–368. [[CrossRef](#)]
39. Gomes, W.J.A.S.; De Oliveira, C.; Huguenin, F. Energy Harvesting by Nickel Prussian Blue Analogue Electrode in Neutralization and Mixing Entropy Batteries. *Langmuir* **2015**, *31*, 8710–8717. [[CrossRef](#)]
40. Ye, M.; Pasta, M.; Xie, X.; Dubrawski, K.L.; Xu, J.; Liu, C.; Cui, Y.; Criddle, C.S. Charge-Free Mixing Entropy Battery Enabled by Low-Cost Electrode Materials. *ACS Omega* **2019**, *4*, 11785–11790. [[CrossRef](#)]
41. Berrettoni, M.; Giorgetti, M.; Zamponi, S.; Conti, P.; Ranganathan, D.; Zanutto, A.; Saladino, M.L.; Caponetti, E. Synthesis and Characterization of Nanostructured Cobalt Hexacyanoferrate. *J. Phys. Chem. C* **2010**, *114*, 6401–6407. [[CrossRef](#)]

42. Kholoud, E.; Watanabe, H.; Takahashi, A.; Emara, M.M.; Abd-El-Nabey, B.A.; Kurihara, M.; Tajima, K.; Kawamoto, T. Cobalt hexacyanoferrate nanoparticles for wet-processed brown-bleached electrochromic devices with hybridization of high spin/low-spin phases. *J. Mater. Chem. C* **2017**, *5*, 8921–8926. [[CrossRef](#)]
43. Martínez-García, R.; Knobel, M.; Balmaseda, J.; Yee-Madeira, H.; Reguera, E. Mixed valence states in cobalt iron cyanide. *J. Phys. Chem. Solids* **2007**, *68*, 290–298. [[CrossRef](#)]
44. Wessells, C.D.; Peddada, S.V.; Huggins, R.A.; Cui, Y. Nickel Hexacyanoferrate Nanoparticle Electrodes For Aqueous Sodium and Potassium Ion Batteries. *Nanoletters* **2011**, *11*, 5421–5425. [[CrossRef](#)]
45. Malecki, G.; Ratuszna, A. Crystal structure of cyanometallates  $\text{Me}_3[\text{Co}(\text{CN})_6]_2$  and  $\text{KMe}[\text{Fe}(\text{CN})_6]$  with  $\text{Me}=\text{Mn}^{2+}$ ,  $\text{Ni}^{2+}$ ,  $\text{Cu}^{2+}$ . *Powder Diffr.* **1999**, *14*, 25–30. [[CrossRef](#)]
46. Loos-Neskovic, C.; Ayrault, S.; Badillo, V.; Jimenez, B.; Garnier, E.; Fedoroff, M.; Jones, D.J.; Merinov, B. Structure of copper-potassium hexacyanoferrate (II) and sorption mechanisms of cesium. *J. Solid State Chem.* **2004**, *177*, 1817–1828. [[CrossRef](#)]
47. Intaranont, N.; Garcia-Araez, N.; Hector, A.L.; Milton, J.A.; Owen, J.R. Selective lithium extraction from brine by chemical reaction with battery materials. *J. Mater. Chem. A* **2014**, *2*, 6374–6377. [[CrossRef](#)]
48. Biendicho, J.J.; West, A.R. Thermally-induced cation disorder in  $\text{LiFePO}_4$ . *Solid State Ionics* **2011**, *203*, 33–36. [[CrossRef](#)]
49. Liu, S.; Fan, C.; Zhang, Y.; Li, C.; You, X. Low-temperature synthesis of  $\text{Na}_2\text{Mn}_5\text{O}_{10}$  for supercapacitor applications. *J. Power Sources* **2011**, *196*, 10502–10506. [[CrossRef](#)]
50. Ghodbane, O.; Pascal, J.; Charles, I.; Montpellier, G.; Cnrs, U.M.R.; Aime, E. Microstructural Effects on Charge-Storage Properties in  $\text{MnO}_2$ -Based Electrochemical. *ACS Appl. Mater. Interfaces* **2009**, *1*, 1130–1139. [[CrossRef](#)]
51. Liu, X.; Zhang, N.; Ni, J.; Gao, L. Improved electrochemical performance of sol-gel method prepared  $\text{Na}_4\text{Mn}_9\text{O}_{18}$  in aqueous hybrid Na-ion supercapacitor. *J. Solid State Electrochem.* **2013**, *1*, 1939–1944. [[CrossRef](#)]
52. Jiang, X.; Sha, Y.; Cai, R.; Shao, Z. The solid-state chelation synthesis of  $\text{LiNi}_{1/3}\text{Co}_{1/3}\text{Mn}_{1/3}\text{O}_2$  as a cathode material for lithium-ion batteries. *J. Mater. Chem. A Mater. Energy Sustain.* **2015**, *00*, 1–9. [[CrossRef](#)]
53. Palacín, M.R. Recent advances in rechargeable battery materials: A chemist's perspective. *Chem. Soc. Rev.* **2009**. [[CrossRef](#)]
54. Meng, J.; Guo, H.; Niu, C.; Zhao, Y.; Xu, L.; Li, Q.; Mai, L. Advances in Structure and Property Optimizations of Battery Electrode Materials. *Joule* **2017**. [[CrossRef](#)]
55. Bro, P.; Marincic, N.; Mallory, P.R.; Science, P. The High Rate Oxidation of Silver Electrodes in Chloride Solutions. *J. Electrochem. Soc.* **1970**, *116*, 1338–1341. [[CrossRef](#)]
56. Jaya, S.; Rao, T.P.; Rao, G.P. Mono- and multilayer formation studies of silver chloride on silver electrodes from chloride-containing solutions. *J. Appl. Electrochem.* **1987**, *17*, 635–640. [[CrossRef](#)]
57. Margalit, N. Cathodes for Seawater Activated Cells. *J. Electrochem. Soc.* **1975**, *122*, 1005–1008. [[CrossRef](#)]
58. Birss, V.I.; Smith, C.K. The anodic behavior the formation and reduction thin silver chloride films. *Electrochim. Acta* **1987**, *32*, 259–268. [[CrossRef](#)]
59. Ha, H.; Payer, J. Electrochimica Acta The effect of silver chloride formation on the kinetics of silver dissolution in chloride solution. *Electrochim. Acta* **2011**, *56*, 2781–2791. [[CrossRef](#)]
60. Jin, X.; Lu, J.; Liu, P.; Tong, H. The electrochemical formation and reduction of a thick  $\text{AgCl}$  deposition layer on a silver substrate. *J. Electroanal. Chem.* **2003**, *542*, 85–96. [[CrossRef](#)]
61. Keramidis, G.; Voutsas, G.P.; Rentzeperis, P.I. The crystal structure of  $\text{BiOCl}$ . *Z. Krist.* **1993**, *205*, 35–40. [[CrossRef](#)]
62. Su, X.; Hatton, T.A. Redox-electrodes for selective electrochemical separations. *Adv. Colloid Interface Sci.* **2017**, *244*, 6–20. [[CrossRef](#)] [[PubMed](#)]
63. Pasta, M.; Wessells, C.D.; Huggins, R.A.; Cui, Y. A high-rate and long cycle life aqueous electrolyte battery for grid-scale energy storage. *Nat. Commun.* **2012**, *3*, 1147–1149. [[CrossRef](#)] [[PubMed](#)]
64. Morais, W.G.; Lima, G.; Gomes, W.J.A.S.; Huguenin, F. Electrochemical Systems for Renewable Energy Conversion from Salinity and Proton Gradients. *J. Brazil Chem. Soc.* **2018**, *29*, 934–947. [[CrossRef](#)]
65. Stejskal, J.; Trchova, M.; Bober, P.; Moravkova, Z.; Kopecky, D.; Vrňata, M.; Prokes, J.; Varga, M.; Watzlova, E. Polypyrrole salts and bases: Superior conductivity of nanotubes and their stability towards the loss of conductivity by deprotonation. *RSC Adv.* **2016**, *6*, 88382–88391. [[CrossRef](#)]
66. Nam, D.; Choi, K. Bismuth as a New Chloride-Storage Electrode Enabling the Construction of a Practical High Capacity Desalination Battery. *J. Am. Chem. Soc.* **2017**, *139*, 11055–11063. [[CrossRef](#)]

67. Musabikha, S.; Ketut Aria Pria Utama, I. Mukhtasor Corrosion in the Marine Renewable Energy: A Review. *Proc. Ocean. Mech. Aerosp.* **2016**, *3*, 121–128.
68. Kristoferson, L.A.; Bokalders, V. Solar Water Distillation. In *Renewable Energy Technologies*; Pergamon: Oxford, UK, 1986; pp. 215–218.
69. Miyai, Y.; Ooi, K.; Katoh, S. Recovery of Lithium from Seawater Using a New Type of Ion-Sieve Adsorbent Based on MgMn<sub>2</sub>O<sub>4</sub>. *Sep. Sci. Technol.* **1988**, *23*, 179–191. [[CrossRef](#)]
70. Liu, M.; Rong, Z.; Malik, R.; Canepa, P.; Jain, A.; Ceder, G.; Persson, K.A. Spinel compounds as multivalent battery cathodes: A systematic evaluation based on ab initio calculations. *Energy Environ. Sci.* **2015**, *8*, 964–974. [[CrossRef](#)]
71. Mao, M.; Gao, T.; Wang, C. A critical review of cathodes for rechargeable Mg batteries. *Chem. Soc. Rev.* **2018**, *47*, 8804–8841. [[CrossRef](#)]
72. Kim, S.; Lee, J.; Kim, C.; Yoon, J. Na<sub>2</sub>FeP<sub>2</sub>O<sub>7</sub> as Novel Material for Hybrid Capacitive Deionization. *Electrochim. Acta* **2016**, *255*, 369–378. [[CrossRef](#)]
73. Huang, Y.; Cheng, F.; Guo, L.; Yang, H.Y. Ultrahigh Performance of Novel Electrochemical Deionization System based on NaTi<sub>2</sub>(PO<sub>4</sub>)<sub>3</sub>/rGo Nanocomposite. *J. Mater. Chem. A* **2017**, *5*, 18157–18165. [[CrossRef](#)]
74. Chen, F.; Huang, Y.; Guo, L.; Ding, M.; Yang, H.Y. A dual-ion electrochemistry deionization system based on AgCl-Na<sub>0.44</sub>MnO<sub>2</sub> electrodes. *Nanoscale* **2017**, *9*, 10101–10108. [[CrossRef](#)] [[PubMed](#)]
75. Guo, L.; Mo, R.; Shi, W.; Huang, Y.; Leong, Z.Y.; Ding, M.; Chen, F.; Yang, H.Y. Prussian blue anode for high performance electrochemical deionization promoted by faradic mechanism. *Nanoscale* **2017**, *9*, 13305–13312. [[CrossRef](#)] [[PubMed](#)]
76. Desai, D.; Beh, E.S.; Sahu, S.K.; Vedharathinam, V.; Van, Q.; De Lannoy, C.; Jose, A.P.; Volkel, A.R.; Rivest, J. Electrochemical Desalination of Seawater and Hypersaline Brines with Coupled Electricity Storage. *ACS Energy Lett.* **2018**, *3*, 375–379. [[CrossRef](#)]
77. Choi, S.; Chang, B.; Kim, S.; Lee, J.; Yoon, J.; Choi, J.W. Battery Electrode Materials with Omnivalent Cation Storage for Fast and Charge-Efficient Ion Removal of Asymmetric Capacitive Deionization. *Adv. Funct. Mater.* **2018**, *1802665*, 1–9. [[CrossRef](#)]
78. Lee, J.; Kim, S.; Kim, C.; Yoon, J. Hybrid capacitive deionization to enhance the desalination performance of capacitive techniques. *Energy Environ. Sci.* **2017**, *00*, 1–7. [[CrossRef](#)]
79. Zhu, X.; Xu, W.; Tan, G.; Wang, Y. Concentration Flow Cells for Efficient Salinity Gradient Energy Recovery with Nanostructured Open Framework Hexacyanoferrate Electrodes. *Energy Technol. Environ. Sci.* **2018**, *3*, 5571–5580. [[CrossRef](#)]
80. Li, G.; Yang, Z.; Jiang, Y.; Jin, C.; Huang, W.; Ding, X. Towards polyvalent ion batteries: A zinc-ion battery based on NASICON. *Nano Energy* **2016**, *25*, 211–217. [[CrossRef](#)]
81. Qu, Q.T.; Shi, Y.; Tian, S.; Chen, Y.H.; Wu, Y.P.; Holze, R. Short communication A new cheap asymmetric aqueous supercapacitor: Activated carbon // NaMnO<sub>2</sub>. *J. Power Sources* **2009**, *194*, 1222–1225. [[CrossRef](#)]
82. Shaz, M.; Van Smaalen, S.; Palatinus, L.; Hoinkis, M.; Klemm, M.; Horn, S.; Claessen, R. Spin-Peierls transition in TiOCl. *Phys. Rev. Lett.* **2005**, *B71*, 100405. [[CrossRef](#)]
83. Gao, P.; Zhao, X.; Zhao-karger, Z.; Diemant, T.; Behm, R.J.; Fichtner, M. Vanadium Oxychloride / Magnesium Electrode Systems for Chloride Ion Batteries. *Appl. Mater. Interfaces* **2014**, *6*, 22430–22435. [[CrossRef](#)] [[PubMed](#)]
84. Gao, P.; Reddy, M.A.; Mu, X.; Diemant, T.; Zhang, L.; Zhao-karger, Z.; Sai, V.; Chakravadhanula, K.; Clemens, O.; Behm, R.J.; et al. Rechargeable Batteries VOCl as a Cathode for Rechargeable Chloride Ion Batteries Angewandte. *Angew. Chem. Int. Ed.* **2016**, *55*, 4285–4290. [[CrossRef](#)] [[PubMed](#)]
85. Zhao, X.; Zhao-karger, Z.; Wang, D.; Fichtner, M. Metal Oxychlorides as Cathode Materials for Chloride Ion Batteries. *Angew. Chem. Int. Ed.* **2013**, *52*, 13621–13624. [[CrossRef](#)]
86. Maguire, J.A.; Banewicz, J.J. Direct Intercalation of Alkali Metal Ions in FeOCl. *Mat. Res. Bull.* **1984**, *19*, 1573–1580. [[CrossRef](#)]
87. Zhao, X.; Li, Q.; Yu, T.; Yang, M.; Fink, K.; Shen, X. Carbon incorporation effects and reaction mechanism of FeOCl cathode materials for chloride ion batteries. *Nat. Publ. Gr.* **2016**, *6*, 1–8. [[CrossRef](#)]
88. Lind, M.D. Refinement of the Crystal Structure of Iron Oxychloride. *Acta Cryst* **1970**, *B26*, 1058–1062. [[CrossRef](#)]

89. El-Halim, A.M.A.; Fawzy, M.H.; Stay, A. Saty Cyclic voltammetric behaviour and some surface characteristics of the lead electrode in aqueous NaCl solutions. *J. Electroanal. Chem.* **1991**, *316*, 275–292. [[CrossRef](#)]
90. Zuo, W.; Zhu, W.; Zhao, D.; Sun, Y.; Li, Y.; Liu, J.; Lou, X.W. Bismuth oxide: A versatile high-capacity electrode material for rechargeable aqueous metal-ion batteries. *Energy Environ. Sci.* **2016**, *9*, 2881–2891. [[CrossRef](#)]



© 2020 by the authors. Licensee MDPI, Basel, Switzerland. This article is an open access article distributed under the terms and conditions of the Creative Commons Attribution (CC BY) license (<http://creativecommons.org/licenses/by/4.0/>).